Oberlin

Digital Commons at Oberlin

Faculty & Staff Scholarship

2-15-2010

Ion microprobe analysis of oxygen isotopes in garnets of complex chemistry

F. Zeb Page
Oberlin College

Noriko T. Kita

John W. Valley

Follow this and additional works at: https://digitalcommons.oberlin.edu/faculty_schol

Part of the Geology Commons

Repository Citation

Ion microprobe analysis of oxygen isotopes in garnets of complex chemistry

F. Zeb Page[1,2], Noriko T. Kita[1], and John W. Valley[1]

[1]Wisc-SIMS
Department of Geoscience
University of Wisconsin – Madison
1215 W. Dayton St.
Madison, WI, 53706, USA

[2]Department of Geology
Oberlin College
52 W. Lorain St.
Oberlin, OH 44074, USA
zeb.page@oberlin.edu
tel: +1 440 775 6701
fax: +1 440 775 8038

REVISED 10/31/09

key words: garnet, oxygen isotopes, SIMS, ion microprobe, Adirondack Mountains, skarn, diffusion

1

2   **Abstract**

3   Accurate ion microprobe analysis of oxygen isotope ratios in garnet is possible if

4   appropriate standards are employed to correct for instrumental bias, a component of which

5   depends on the cation chemistry of the analyzed mineral. In this study, 26 garnet standards

6   (including 14 new standards) that span the compositional range of pyrope, almandine,

7   grossular, spessartine, and andradite were analyzed repeatedly by ion microprobe to develop

8   a new method of correcting for instrumental bias in garnets. All analyses were normalized to

9   a single master garnet standard (*UWG-2*) before bias from cation composition was

10   considered. Bias due to cation composition in garnet was found to correlate with grossular

11   content in pyralspite garnets and with andradite in ugrandite garnets. Bias is correlated with

12   molar volume in garnets of all compositions in this study. Although this correlation is

13   suitable as a correction scheme for bias, a more accurate correction scheme based on the

14   grossular and andradite compositions of garnet is proposed. This method reproduces the bias

15   of all but one standard to within a range of 0.4‰, an accuracy that is on the same order as the

16   reproducibility (±0.3‰, 2 S.D.) of the master garnet standard *UWG-2*, but that remains an

17   independent source of error. The new correction scheme is used to successfully reproduce

18   laser fluorination analyses along a traverse of a polymetamorphic, zoned skarn garnet from

19   the Adirondack Mountains. While previous analyses were at the mm-scale, the new data

20   resolve a gradient of $\delta^{18}O$ of 2.1‰ over 16 μm. If experimentally derived diffusion

21   coefficients are correct, these new results show that granulite-facies metamorphism was

22   significantly faster than previously assumed and the thermal peak was less than 5 Myr.

23

24

1. Introduction

Metamorphism in hydrothermal systems or skarns is often accompanied by radical shifts in fluid composition and temperature over short time scales (e.g., Taylor and O'Neil, 1977; Bowman, 1998). In response to these changes, garnets and other minerals may form oscillatory zoning patterns in their major and trace element chemistry (e.g., Yardley et al., 1991; Jamtveit et al., 1993) as well as their oxygen isotope ratios (e.g., Clechenko and Valley, 2003). These micro-scale chemical and isotopic variations can be used to reconstruct ancient metamorphic fluid regimes. In particular, the oxygen isotope ratio of metamorphic garnet is a powerful tracer of hydrothermal systems because of the strong isotopic contrast between meteoric and most magmatic fluids (Valley, 1986) and the ability of garnet to preserve these ratios because of slow intragranular diffusion (e.g., Coghlan, 1990; Lancaster et al., 2009). However, the scale of isotopic heterogeneity within skarn minerals is generally much smaller that the volume of material required for analysis by conventional methods. Because of this, skarn garnets are an excellent target for oxygen isotope analysis by ion microprobe, and two studies have used single-collector ion microprobes to show that garnets preserve a detailed oxygen isotopic record of hydrothermal fluid history (Jamtveit and Hervig, 1994; Crowe et al., 2001).

The most recent generation of multicollector ion microprobes has allowed significant advances for in situ oxygen isotope analysis both in terms of reduced analysis spot size and in analytical precision. Analyses of minerals with limited cation solid solution, such as zircon and quartz, have improved from ± 2‰ (2 S.D.) on 30 µm diameter pits (e.g., Valley and Graham, 1991) to ± 0.7‰ (2 S.D.) on 20 µm pits (Cavosie et al., 2005) to ± 0.3‰ (2 S.D.) on 10 µm pits (Kelly et al., 2007; Kita et al., 2009; Valley and Kita; 2009). For ultra-small spots

48   (< 1µm in diameter) Page et al. (2007) attained a precision of ± 2‰ (2 S.D.). The smaller

49   spot sizes and better precision can be attributed to improvements in technology and to

50   refinements in technique, which include tuning and operation of the instrument, sample

51   preparation, and standardization (Kita et al., 2009; Valley and Kita, 2009). For some

52   minerals, including magnetite and hematite, the orientation of the crystal lattice has been

53   shown to affect the instrument bias (Huberty et al. 2009), however, the data reported here

54   show that any such orientation effect is smaller than the grain-to-grain precision of ±0.3‰

55   that is regularly attained for randomly orientated grains of garnet. Due to the significant

56   instrument bias inherent in ion microprobe analysis (e.g., Shimizu and Hart, 1982), accurate

57   measurements of stable isotope ratios must be empirically corrected by regular and frequent

58   analysis of well-characterized reference material. Because variable cation composition of

59   some minerals or glasses contributes to the instrumental bias (the "matrix effect" or

60   instrumental mass fractionation e.g., Eiler et al., 1997; Valley and Kita, 2009), most ion

61   microprobe studies of oxygen isotope ratios have been confined to phases of limited solid

62   solution (e.g., zircon, quartz, calcite). In addition, many papers that address instrumental bias

63   and propose correction schemes were developed for a previous generation of single-collector

64   ion microprobes that made use of extreme energy filtering with only one collector and

65   relatively low mass resolution (e.g., Hervig et al., 1992; Riciputi and Paterson, 1994; Eiler et

66   al., 1997; Riciputi et al., 1998). Under these conditions, the instrumental bias can be in

67   excess of 50‰ for $\delta^{18}O$. More recently, Vielzeuf et al. (2005a) addressed the issue of bias in

68   a large-radius multicollector ion microprobe, specifically in aluminous Fe^{2+}-Mg-Ca garnets,

69   and developed a new correction scheme to allow relatively accurate analyses of these

70   compositions (± 1-2‰, 30-50µm pits). The instrument bias for these analyses at high mass-

71 resolution (MRP~2500) and low energy offset was significantly lower, below 7‰. The

72 cation compositional range of the standards introduced by Vielzeuf et al. (2005a) are

73 sufficient to address the instrumental bias in Al-rich Fe^{2+}-Mg-Ca (pyralspite) garnets

74 commonly found in metasedimentary, metamafic, and some igneous rocks. There are several

75 studies that have established oxygen isotope zoning in garnets of these compositions (e.g.,

76 Kohn et al., 1993, 1994, 1997; Skelton et al., 2002; Peck and Valley, 2004) and some that

77 have made use of ion microprobe analysis of zoned pyralspite garnets (Vielzeuf et al.,

78 2005a,b; Martin et al., 2006; Lancaster et al., 2009). However, hydrothermal skarn garnets

79 are most commonly Ca-rich with variable Fe^{3+}/Al (ugrandite) and the Vielzeuf et al. (2005a)

80 standard set and correction scheme does not extend to these compositions.

81 The present study uses new, higher precision analyses by the latest generation

82 multicollector ion microprobe (ims-1280) to examine instrumental bias systematically from

83 26 garnet standards covering a wide range of solid solution, including more Ca-rich grossular

84 and andradite compositions. This study has three main goals: 1) to increase the range of

85 possible applications of this method; 2) to develop more straightforward, flexible and

86 accurate correction schemes; and 3) to use these methods to place constraints on the rate of

87 oxygen diffusion in garnet. We have applied our new correction procedure in the analysis of

88 an oscillatory-zoned garnet from the Willsboro Mine, a polymetamorphosed garnet-diopside-

89 wollastonite skarn from the Adirondack Mountains, New York, USA, described by

90 Clechenko and Valley (2003).

91

92 **2. Garnet Standards**

93   In this study, 27 garnet standards were used to evaluate matrix effects in oxygen

94   isotope analysis by ion microprobe (Table 1). All of these standards were evaluated for

95   oxygen isotopic homogeneity by ion microprobe, and for cation homogeneity by electron

96   microprobe (Supplementary Table A). Oxygen isotope ratios were determined by laser

97   fluorination for all new standards, and in some cases existing standards were analyzed as

98   well for comparison to values in the literature. The standards used in this study and their

99   average cation and isotopic compositions and observed isotopic variability are recorded in

100   Table 1; cation compositions are shown in Figure 1; electron microprobe analyses, cation

101   variability and formula calculation are found in Table A, supplementary electronic materials.

102   Five garnet standards (Fig. 1) from Eiler et al. (1997) provide near-end-member

103   compositions for grossular (*GrsSE*) and spessartine (*SpsSE*) garnets as well as slightly more

104   dilute almandine (*AlmSE* & *AlmCMG*), and one intermediate almandine-pyrope (*UWG-2*)

105   that is an extremely well-characterized standard for laser fluorination analysis of $\delta^{18}O$

106   (Valley et al., 1995). Vielzeuf et al. (2005a) increased the cation compositional range of ion

107   microprobe garnet standards, particularly along the pyrope-almandine join by including an

108   end-member pyrope from the Dora Maira quartzite (*PypDM*) and five more intermediate

109   compositions (*PypMM, PypAk, PypAA, Bal509, β114).* In addition, they included one more

110   standard on the almandine-grossular join (*2B3*). Detailed information on the origins of these

111   standards as well as chemical composition and unit cell dimensions can be found in Vielzeuf

112   et al. (2005a).

113   In addition to these existing standards, we introduce 6 garnet standards from eclogitic

114   xenoliths in kimberlite with intermediate almandine – pyrope compositions and from 7 to 61

115   mol % grossular. Standards *13-63-21, 13-62-27, 13-62-29, 13-63-20,* and *13-63-44* were

116   separated by Dan Schulze from xenoliths found in the Blaauwbosch kimberlite, South Africa

117   (Ford, 1987; Schulze et al., 2003). Standard *R-53* is from an eclogitic xenolith found in the

118   Roberts-Victor kimberlite (Garlick et al., 1971; MacGregor and Manton, 1986). To

119   supplement the grossular-rich standard (*GrsSE*) used by both Eiler et al. (1997) and Vielzeuf

120   et al. (2005a), we introduce three more grossular-rich garnets (*92W-1, 10691, AF749A)* from

121   garnet-diopside-wollastonite skarn metamorphosed to the granulite faces (Willsboro-Lewis

122   skarn belt, Adirondack Mts., Kohn and Valley, 1998). An additional grossular-rich sample,

123   *MexGrs* (Riciputi et al. 1998) was also analyzed but was excluded from the standard set

124   because of numerous inclusions. Finally, to investigate matrix effects on the grossular-

125   andradite join, we include four more standards (*92Lew-2, 92Lew-7, 92Lew-8, 92Lew-10*)

126   with the compositional range And_{49-91}, from the same skarn belt (Kohn and Valley, 1998).

127

128   **3. Analytical Methods**

129   *3.1 Sample Preparation*

130   Garnet standards were crushed by hand, cast in 25 mm epoxy disks, and polished. All

131   garnet standards and samples were mounted within 5 mm of the center of the epoxy disk, and

132   all mounts include multiple grains of the *UWG-2* standard at the center of the mount.

133   Standards vary in grain size from ~150 μm to up to 5 mm, depending on the nature of the

134   source material; between 3 and 36 grains of each standard were mounted in standard blocks.

135   A zoned grossular-andradite garnet from the Willsboro wollastonite skarn (Adirondack

136   Highlands, New York) that was previously analyzed for traverses of $\delta^{18}O$ at mm-scale by

137   laser fluorination (garnet 1a of Clechenko and Valley, 2003) using a thin saw-blade

138   technique (Elsenheimer and Valley, 1993) was also prepared for ion microprobe analysis.

139   The Willsboro sample consists of a 700 μm thick polished wafer of rock (thick section)

140   attached to a glass microscope slide with superglue from which a ~1 mm wide strip of

141   material that represents a core to rim garnet transect had been removed and analyzed in chips

142   by laser fluorination. The portion of the garnet immediately adjacent to this transect was

143   removed from the slide with acetone and cast in the center of an epoxy disk containing the

144   *UWG-2* standard and repolished for ion microprobe analysis.

145   *3.2 Electron Microprobe*

146   Cation chemistry of garnets was determined using the CAMECA SX51 electron

147   microprobe at the University of Wisconsin - Madison. Garnets were analyzed in point beam

148   mode with an accelerating potential of 15 kV and 20 nA beam current. The counting time

149   was 10s on peak and 5s on both sides, off-peak. Natural and synthetic silicate and oxide

150   standards were used. Data were reduced using the Probe for Windows software (Donovan et

151   al., 2007), and oxygen was calculated by stochiometry. Fe^{2+}/Fe^{3+} was estimated by charge-

152   balance, assuming no site vacancies or OH substitution (Afifi and Essene, 1988). Chemical

153   analyses of all garnet standards are presented in Supplementary Table A and summarized in

154   Table 1.

155   *3.3 Laser Fluorination*

156   Analysis of oxygen isotopes to calibrate ion microprobe analyses for new standard

157   material was performed on 1-2 mg garnet chips that were treated overnight at room

158   temperature in the sample chamber with BrF_5, then individually heated with a CO_2 laser in

159   the presence of BrF_5 to release O_2, which was cryogenically purified, converted into CO_2,

160   and analyzed on a Finnigan MAT 251 mass spectrometer (Valley et al., 1995). Isotopic ratios

161   are reported in per mil (‰) notation relative to standard mean ocean water (VSMOW).

162 Accuracy and analytical precision were verified during each session by multiple analyses of

163 the garnet standard *UWG-2* (Valley et al., 1995). Raw standard $\delta^{18}O$ values for each session

164 were corrected to the accepted UWG-2 value ($\delta^{18}O$ = 5.80‰ VSMOW) and the same

165 correction was applied to samples. The average uncorrected $\delta^{18}O$ value ($\pm$ 2 S.D.) of UWG-2

166 was 5.59 $\pm$ 0.08‰ (n=5).

167 *3.4 Ion Microprobe*

168 *3.4.1 Analysis Conditions*

169   Oxygen isotopic analyses were performed on the WiscSIMS CAMECA ims-1280

170 high-resolution, multi-collector ion microprobe at the University of Wisconsin – Madison in

171 10 analytical sessions over the course of over 2 years. A $^{133}Cs^+$ primary ion beam (20 kV

172 total accelerating voltage) was focused to a diameter of 10 μm on the gold-coated sample

173 surface. Secondary O^- ions were accelerated away from the sample by −10 kV and the

174 analysis site was centered under a uniform electron field generated by a normal-incidence

175 electron gun for charge compensation. Primary ion intensities were ca. 2-3 nA. The

176 secondary ion optics were configured similarly to those reported in Kita et al. (2009) in order

177 to achieve high secondary ion transmission. Instrument parameters include: transfer lens

178 magnification of 200, contrast aperture (CA) 400 μm diameter, field aperture (FA) 4000 x

179 4000 μm square, entrance slit width 122 μm, energy slit width 40 eV, and exit slit width

180 500μm. At these conditions, both the primary ion spot image transferred to the FA window

181 and the crossover image through the CA and entrance slit were almost fully transmitted

182 compared to fully opened conditions. The intensity of ^{16}O was 2 to 3 x10^9 cps depending on

183 the primary intensity (ca. 10^9 cps/nA). Mass resolving power (MRP, M/ΔM), measured at

184 10% peak height, was set to ca. 2200, enough to separate hydride interferences on ^{18}O. Two

185   Faraday cups (FC) were used to measure ^{16}O and ^{18}O simultaneously and the amplifiers on

186   each were equipped with 10^{10} and 10^{11} Ω resistors, respectively. The base line of the FC

187   amplifiers was measured at the beginning of each analytical session; drift during the day was

188   insignificant compared to the noise level of the detectors (≤1000 cps for the ^{18}O FC with 10^{11}

189   Ω resistor, Kita et al., 2009). The magnetic field was regulated by a Nuclear Magnetic

190   Resonance (NMR) probe with stability of mass better than 10 ppm/10 hours. At each analysis

191   position, any small misalignment of the secondary optics due to changing stage position was

192   automatically re-tuned before analysis. Instrument stability during each analytical session is

193   documented by repeated analyses of the UWG-2 standard (Supplementary Table B).

194   *3.4.2 Standardization*

195   Minerals with limited solid solution (e.g., quartz, calcite, zircon) are corrected for

196   instrument bias by adjusting the raw data by a factor ($\alpha^{18}O_{SIMS}$) obtained by analyzing a

197   standard of the same mineral and chemical composition embedded in the same mount.

198   Blocks of typically 4 standard analyses (different spots on one or more grains) are made

199   before and after each set of sample analyses. In order to isolate the variation of bias

200   generated by matrix effects within the garnet family from other sources of bias such as

201   variability of instrument conditions over time, raw data from all garnet analyses (sample and

202   compositional standard) were first corrected using the bracketing analyses of the *UWG-2*

203   standard that is embedded in each sample mount. A fractionation factor ($\alpha^{18}O*_{SIMS}$) is

204   calculated from the bracketing analyses of *UWG*-2 relative to the accepted value of *UWG-2*

205   on the VSMOW scale (5.80‰, Valley et al., 1995) following equation 2.1 in Kita et al.

206   (2009).

207

208 $$\alpha^{18}O*_{SIMS} = \frac{1 + \left(\delta^{18}O_{RAW}/1000\right)}{1 + \left(\delta^{18}O_{VSMOW}/1000\right)}$$ (3.1)

209 A preliminary $\delta^{18}O$ value for each sample (or compositional standard) is then

210 calculated using $\alpha^{18}O*_{SIMS}$ and equation 2.5 of Kita et al. (2009).

211 $$\delta^{18}O* = \left\{\left[1 + \left(\delta^{18}O_{RAW}/1000\right)\right]/\alpha^{18}O*_{SIMS} - 1\right\} \times 1000$$ (3.2)

212 This preliminary corrected value is denoted as $\delta^{18}O*$ and is the same as $\delta^{18}O_{VSMOW}$

213 only for garnets with the same bias (or chemical composition) as *UWG-2* and $\delta^{18}O*$

214 increasingly differs from the VSMOW scale as garnet compositions (and biases) differ from

215 that of *UWG-2*. The use of a preliminary correction to $\delta^{18}O*$ allows comparison of data

216 between standard brackets or between different analysis sessions, but does not take into

217 account the bias generated by chemical variability among garnets. This bias observed in the

218 25 other (secondary) garnet standards (vs. UWG-2) can be expressed in permil deviation

219 from the bias observed in the analysis of *UWG-2* with the following relation:

220 (bias rel. *UWG-2*) $\approx \delta^{18}O* - \delta^{18}O$ (3.3)

221 where $\delta^{18}O$ is the isotopic composition of the standard on the VSMOW scale as determined

222 by laser fluorination. Because the bias, $\delta^{18}O*$ and $\delta^{18}O$ generally differ by less than 10‰

223 (and in most cases, they differ by much less) this approximation is accurate to within 0.1‰

224 (Kita et al. 2009).

225 For analyses of sample garnets, a correction is applied based on the compositional

226 dependence of bias observed among standards analyzed during the same analysis session.

227 Different possible correction schemes are compared in section 5.4. In addition to isolating

228 compositional effects from other sources of bias, this correction method allows us to use a

229 single, particularly well-characterized standard (*UWG-2*) to evaluate spot-to-spot

11

230   reproducibility of analyses by emulating the standard-sample-standard bracketing correction

231   schemes used to ensure high precision and accuracy oxygen isotopic analyses of other phases

232   such as zircon, calcite, and quartz. Finally, using *UWG-2* as a "master standard" allows a

233   significant practical advantage in that only one standard need be embedded in each sample

234   mount, and other standard material used to evaluate or correct for matrix bias can be reused

235   in separate standard mounts as long as they are also corrected to *UWG-2*. The external errors

236   of bracketing *UWG-2* analyses were typically 0.2-0.4‰ (2 S.D.) for 10μm diameter analysis

237   pits. After ion microprobe analysis, the bottoms of all pits were examined by scanning

238   electron microscope in secondary electron imaging for inclusions and cracks that might affect

239   the measured oxygen isotope ratios, and classified as "regular" or "irregular" according to

240   Cavosie *et al.* (2005). All data used in this study are exclusively from pits that were observed

241   to be "regular" (inclusion and crack-free).

242   *3.4.3 Sputter test*

243   Eiler et al. (1997) observed a strong correlation with a single collector ion microprobe

244   between the bias and sputter rate of glasses of various compositions and albite, and used this

245   correlation as the foundation of a kinetic model to predict matrix effect bias. To compare the

246   sputter rate of sample material with instrument bias, we conducted a sputtering rate test on a

247   subset of garnet standards. The primary Cs^+ ion beam was focused into a point beam and

248   rastered over a 30 x 30 μm region for 60 minutes. The dimensions of the pits were measured

249   at nm-scale using a Zygo white-light profilometer. The rastered pits were found to have flat

250   bottoms, and the depth was by taken as the average depth of the center portion of four

251   transects through the center of each square pit. The reproducibility of this measurement was

252   on the order of 2-3 nm for a single pit.

253

4. Results

255   Garnet standards were analyzed in ten sessions from April 2006 to August 2008, with

256   between 3 and 25 standards analyzed per session. Each standard was analyzed between 4 and

257   20 times per session and bias data were corrected by the average bias calculated from the

258   bracketing *UWG-2* analyses. Instrumental bias measured on *UWG-2* ranged from 1.5 to

259   4.6‰ between analysis sessions, but varied by less than 0.6‰ within a single session

260   (average reproducibility = ±0.3‰ 2 S.D.). Spot to spot reproducibility of secondary standards

261   ranges from ±0.2 to ±0.8‰ (2 S.D.) with an average reproducibility of 0.4‰ (2 S.D., Table

262   1). More than half of the standards, spanning the entire compositional range, displayed

263   variability on the same order as the analytical uncertainty ($\leq$ 0.4‰, 2 S.D.). The observed

264   variability in a number of standards greater that analytical uncertainty is likely due to some

265   small degree of natural heterogeneity. The bias relative to *UWG-2* for each standard in each

266   session is reported in Table 2, and detailed data from each analysis session can be found in

267   Table B of the electronic supplementary materials. When standards were analyzed multiple

268   times over the 28-month period, bias relative to *UWG-2* was found to vary on average by

269   ±0.3‰ and in all cases less than ±0.7‰.

270   The component of instrumental bias caused by matrix effects (i.e., bias rel. to *UWG-

271   2*) of garnet standards in this study ranges from -1.1‰ for near end-member pyrope and

272   almandine standards to +7.1‰ for the most andradite-rich standard. Low-Ca (grossular +

273   andradite < 20 mol%) standards (pyrope, almandine, and the single spessartine) have a very

274   limited range of bias (1.5‰) out of the total range of 8.2‰. In Al-rich, Mg-Fe^{2+}-Ca garnets,

275   bias ranges 4‰ (-1.1 to +2.9‰ relative to *UWG-2*) and correlates with the grossular content

276   (Fig. 2a) as previously described by Vielzeuf et al. (2005a). However, in grossular-andradite

277   garnets bias ranges an additional 4.2‰ (+2.9 to +7.1‰ relative to *UWG-2*) and is inversely

278   correlated with the grossular content (Fig. 2b) and positively correlated with the andradite

279   content. Data from the sputter test are presented in Table C and are plotted in Figure A of the

280   electronic supplementary materials; no correlation was found between sputter rate and bias

281   for garnets, in contrast to single detector data at high energy offset for albite and silicate

282   glasses (Eiler et al., 1997).

5. Discussion

5.1 Comparison with previous work

285   There is a broad correlation in the magnitude and sign of instrumental biases among

286   standards of similar composition used in this study and Vielzeuf et al. (2005a). However,

287   there are significant differences in the measured bias values between the two studies. The

288   total range in bias varies up to 6.3‰ in Vielzeuf et al. (2005a) but varies only 4.0‰ over the

289   same compositional range in this study. The bias on *UWG-2* ranges between 1.5 and 4.6‰

290   between analysis sessions in this study, whereas it varies from -4.8 to 0.5‰ in Vielzeuf et al.

291   (2005a). Although the different ranges of UWG-2 values (range = 3.1 vs. 5.3‰) suggests

292   greater variability in instrument conditions in one study, the differences in bias between the

293   two multicollector ion microprobe studies are small when compared with the -60.4‰ bias

294   generated by the analysis of *UWG-2* on a single collector ion microprobe at high energy

295   offset (Eiler et al., 1997). A more detailed comparison between the present study and that of

296   Vielzeuf et al. (2005a) is somewhat confounded by different standardization techniques.

297   Vielzeuf et al. (2005a) did not run a specific standard (such as *UWG-2*) as frequently as in

298   this study to correct for small instrumental drifts and simply reported instrumental bias for

299   each standard relative to the VSMOW scale. Because of this, measurements of instrumental

300   bias for every garnet standard (*UWG-2* and other standards) within and among analysis

301   sessions include changes in instrumental conditions and may not be directly compared.

302   *5.2 Bias and garnet composition*

303   Instrument bias in garnets is strongly correlated with Ca-content in Al-rich garnets

304   and appears to be approximately linear for compositions of less than ~30 mol.% grossular

305   (Fig. 2a). However, compositions of greater than 30 mol.% grossular affect bias to a lesser

306   degree. Bias changes ~ 2‰ relative to *UWG-2* between 0-30 mol.% grossular, but only

307   increases an additional ~2‰ between 30-90 mol.% grossular. This non-linear relationship

308   between bias and composition is consistent with similar trends observed in feldspars,

309   pyroxenes, olivine, and carbonates (Valley and Kita, 2009) In Ca-rich garnets, bias is

310   inversely correlated with grossular (Al) content (Fig. 2b) and positively correlated with

311   andradite (Fe^{3+}), with one clear outlier (*MexGrs*). The instrumental bias measured for

312   *MexGrs* is consistently > 1‰ greater than the four other grossular-rich garnets of similar

313   composition in this study. Ion microprobe analyses of *MexGrs* suggest that the garnet itself is

314   not strongly variable in oxygen isotopic composition (±0.7‰ 2 S.D.). However, unlike any

315   other garnet in this study, *MexGrs* contains a substantial number of inclusions. Although

316   these inclusions are easy to avoid with the ion microprobe, the calibration by laser

317   fluorination analysis constitutes a mixture of garnet and inclusion material. For this reason

318   we exclude *MexGrs* as a standard material in our calibration, although we show the data for

319   completeness.

320   Vielzeuf et al. (2005a) recognized a correlation between the Ca content of Al-rich

321   garnets and bias in most of their analysis sessions. This observation is largely based on one

322   Ca-rich standard (*GrsSE*). The addition of more Ca-rich standards in this study confirms the

323   strong correlation between Ca (grossular) and bias, and indicates that Fe^{+3} (andradite) has an

324   even stronger effect on instrumental bias.

325   *5.3 Bias and molar volume*

326   Andradite and grossular have a substantially larger unit cell dimension than the other

327   garnet end-members in this study. In order to test a correlation between molar volume and

328   instrument bias (a possibility proposed by Vielzeuf et al., 2005a), the molar volume of each

329   garnet standard was estimated as a weighted average of the molar volumes of end-members

330   assuming ideal mixing. Volume data for pyrope, almandine, grossular, and andradite are

331   taken from Robie and Hemingway (1995) and volume data for spessartine and uvarovite are

332   from Diella et al. (2004). Physical properties of garnet such as unit cell dimension have long

333   been successfully approximated from chemical data (e.g., Novak and Gibbs, 1971). The

334   calculated molar volume for each standard can be found in Table 1, and agree well with the

335   molar volumes determined for the subset of standards with published volumes determined by

336   X-ray diffraction (Vielzeuf et al. 2005a).

337   The instrumental bias for the garnet standards in this study is well correlated with the

338   calculated molar volume (Fig. 3). A least-squares linear regression of the data for all 26

339   standards (excluding MexGrs) yields an R^2 value of 0.95. However, there is substantial

340   variability of the data about the best-fit line, greater than the degree of observed

341   heterogeneity in both cation and isotopic composition of the garnet standards. As in the study

342   of Vielzeuf et al. (2005a), the lone spessartine-rich standard (*SpsSE*) lies well below the

343   correlation between molar volume and bias line. However, *SpsSE* is not an outlier in the

344   correlation between grossular and bias among Al-rich garnets (Fig. 2a).

345   Although the correlation between molar volume and bias provides a simple linear

346   relationship, it does not explain the relatively large degree of variability observed among

347   standards of similar cation composition, particularly those rich in grossular (even without

348   *MexGrs*). One possibility in the case of greater observed bias than that predicted by

349   calculated molar volume is the presence of an end-member such as hydrogrossular or

350   hydroandradite that is analytically difficult to measure, but has a strong effect on molar

351   volume. However, there is no evidence of a significant detectable hydrogen-bearing

352   component (in the form of silica deficiency) for any of these standards. Although molar

353   volume may provide a strong control on bias, one or more additional second-order effects

354   may be responsible for the observed variability.

355   *5.4 Correction scheme*

356   Correlations between physical properties and instrumental bias have been reported

357   before (Hervig et al. 1992, Eiler et al. 1997, Riciputi et al. 1998). These workers noted a

358   correlation between atomic mass and bias but also observed that the presence of residuals of

359   up to 10‰ made this correlation unsuitable as a correction scheme. Most recently, Vielzeuf

360   et al. (2005a) reported a correlation between molar volume and bias for garnets. However,

361   because of limited standards, this correlation was deemed unsuitable as the basis for a

362   correction scheme.

363   With the increased number of standards in this study, the observed correlation

364   between calculated molar volume and bias could be used as a basis for correction. A least-

365   squares linear regression of the data for 25 standards (not including the 2σ *SpsSE*) yields the

366   relation:

367   Bias (‰ relative to UWG-2) = 0.426 x calc. molar volume (cc/mol) - 49.42   (5.1)

368 with an R^2 value of 0.97 (2 S.E. of the estimate = 0.88‰). This represents a substantial

369 improvement in comparison to the correction scheme of Vielzeuf et al. (2005a) that was

370 based on a linear interpolation of the bias of four standards that bracket the sample in

371 almandine, pyrope, grossular, and spessartine content. The relation between bias and molar

372 volume described by equation (5.1) reproduces the measured composition of 75% of the 25

373 standards used to within ±0.5‰ of their accepted value, 85% to within ±0.6‰, and 95% to

374 within 0.7‰. Despite the extension in compositional range offered by this correction scheme,

375 the improvement in accuracy (± 0.88‰ 2 S.E. of the estimate based on 25 garnets) is still

376 substantially worse that the precision of the method as evidenced by typical reproducibility

377 of standard analyses on the order of ±0.4‰ (2 S.D.).

378   Another possible correction scheme is based on compositional variables, particularly

379 the strong correlation between bias and grossular content in pyralspite garnets and andradite

380 in ugrandite garnets. Riciputi et al. (1998) showed that instrumental bias in grossular-

381 andradite garnets in single-collector ion microprobes could be estimated using a linear

382 interpolation of bias along the Al-Fe^{3+} chemical join, and suggested that this be the basis of a

383 correction scheme. In this study, the relationships between bias and grossular among

384 pyralspite garnets and between bias and andradite in ugrandite garnets are non-linear (Fig. 4).

385 However, both are well-modeled with simple polynomial functions, with far less variability

386 than the linear regression between molar volume and bias. This non-linear relationship is

387 similar to that observed among other silicates and carbonates (Valley and Kita, 2009). The

388 instrumental bias of the nineteen standards with less than 5 mol.% andradite (including

389 *SpsSE*) can be related to the mole fraction of grossular (+minor uvarovite) with the following

390 relation:

391   Bias (‰ relative to UWG-2) = -5.04$(X_{Grs+Uvar})^2$ + 8.96$(X_{Grs+Uvar})$ - 1.09   (5.2)

392   For the 8 garnet standards (excluding *MexGrs*) that contain less than 10% almandine +

393   pyrope + grossular, bias can be related to andradite (+ minor CaTi garnet) as

394   Bias (‰ relative to UWG-2) = -1.92$(X_{And+CaTi})^2$ + 6.18$(X_{And+CaTi})$ - 2.87   (5.3)

395   These two calibrations reproduce the actual compositions of the 26 garnet standards used to

396   ± 0.40‰ (2 S.E. of the estimate), a substantial improvement to the molar volume correction

397   that makes accuracy comparable to the reproducibility of most garnet standards.

398   It is important to stress that the calibrations above are presented to demonstrate and

399   compare between methods of correction. The values of instrumental bias measured relative to

400   *UWG-2* for each standard remain remarkably consistent between analysis sessions, but

401   should in no way be the basis for correction of data collected on different instruments under

402   different operating conditions. New calibration curves should be generated by users on their

403   own instruments, ideally during the same analysis session as the samples to be corrected. The

404   use of a calibration based on 26 garnet standards (or even a substantial subset thereof) that

405   need to be analyzed during each analysis session is impractical for routine correction of

406   garnet data. A more practical approach to a correction scheme correction is to use a subset of

407   standards that compositionally bracket the unknown and then estimate bias based on the

408   grossular or andradite composition as appropriate. Our preferred correction procedure is a

409   calibration curve based on grossular or andradite composition. At least 3-4 standards are

410   analyzed that bracket the chemical composition of the unknown sample and delineate the

411   overall shape of the curve (e.g., both low and high grossular/andradite standards are included

412   in each calibration to avoid artifacts that might arise from a quadratic equation fit to only

413   three points over a narrow compositional range). Compositional standards should be

19

414   analyzed during the same analysis session as samples to be corrected. A number of

415   calibration curves were generated based on 3-4 standards using this approach. As long as the

416   standards were chosen to cover a broad range of grossular or andradite compositions, the

417   calibrations reproduced the full 26 garnet standard set to within ± 0.3-0.5‰ (2 S.E. of the

418   estimate). This approach yields similar accuracy to that achieved with use of all standards.

419   The use of a correction procedure in which all samples are first normalized to *UWG-2*

420   to correct for any instrumental instability and then corrected for matrix effect bias using the

421   grossular or andradite of at least 3 secondary standards that compositionally bracket the

422   unknown offers significant advantages in precision, accuracy, and convenience. Correction to

423   a master standard allows for a single consistent method of determining the precision

424   (reproducibility) of analyses as well as the practical advantage of allowing compositional

425   standards to be stored in standard mounts and not embedded with samples. This allows use of

426   the best and most plentiful standard for all sample mounts, and conserves more precious

427   materials.

428   Errors in ion microprobe analyses arise from a myriad of sources ranging from

429   counting statistics to sample topography (e.g., Kita et al., 2009). Propagation of all these

430   sources of error would be an extremely arduous undertaking, and for this reason the external

431   reproducibility of a standard is the best (and most workable) metric for error estimation

432   (Valley and Kita, 2009). An instrumental bias calibration that is dependant on compositional

433   variables introduces a new source of error independent of that measured by standard

434   reproducibility. Errors resulting from the calibration scheme must therefore be added in

435   quadrature to those arising from analytical uncertainty. However, it should be noted that the

436   proposed calibration does not fully explain all sources of instrumental bias just as counting

437   statistics do not encompass all other sources of error in an analysis. True statistical rigor in

438   the treatment of these uncertainties is, as yet, impossible.

439

440   **6. Application to growth zoning and diffusion**

441   *6.1 Adirondack skarn garnet*

442   The Adirondack Mountains of New York, USA are a Mid-Proterozoic,

443   polymetamorphic, granulite-facies orogenic terrane. Intrusion of anorthosite and related

444   magmas (1155±5 Ma, McLelland et al., 2004) formed a contact metamorphic aureole

445   including skarn rocks that predate the peak of regional metamorphism (Valley and O'Neil,

446   1982; Valley, 1985; Valley et al., 1990). The Adirondack skarns were buried and largely

447   recrystallized during the Ottawan (ca. 1050 Ma) regional granulite-facies metamorphism, but

448   small domains of unrecrystallized, oscillatory-zoned skarn garnets were locally preserved at

449   the Willsboro Mine. Clechenko and Valley (2003) analyzed the oxygen isotopic composition

450   of one to two centimeter diameter zoned garnets from Willsboro by laser fluorination of mm-

451   scale chips taken from a core to rim transect of the garnets removed with a thin diamond saw.

452   The oxygen isotopic composition of this transect in combination with major and trace

453   element data were used to infer variable mixing of metamorphic fluids from meteoric (low

454     $\delta^{18}O$, Ca-rich) and magmatic (high $\delta^{18}O$, Fe-rich) sources. The garnet zoning was preserved

455   through subsequent granulite-faces metamorphism.

456   In this study we analyze oxygen isotope ratios along a traverse in one of the garnets

457   (garnet 1a) previously analyzed by Clechenko and Valley (2003) collected from the

458   Willsboro Mine, NY, USA (approx. 44˚18'52"N, 73˚52'54"W) in order to assess the

459   accuracy of our correction technique, as well as to search for finer-scale isotopic zoning and

21

460 possibly larger variation than could be resolved by the existing analyses. The previous laser

461 fluorination data document gradients in $\delta^{18}O$ of ~ 3‰ over 1 mm, but larger and sharper

462 gradients are predicted for contact metamorphism. The new ion microprobe data interrogate

463 these gradients at a scale that is up to 100 times finer in linear resolution and one million

464 times smaller in volume.

465 *6.2 Analysis and correction*

466 The remainder of the polished section of garnet 1a of Clechenko and Valley (2003)

467 was mounted in epoxy with standard *UWG-2* and repolished. The original Fe-Kα X-ray map

468 of the composition of this garnet is reproduced in Figure 5a with the location of the laser-

469 fluorination traverse and the new ion microprobe traverse. The traverse in this study was

470 located adjacent to and parallel with the previous traverse. Seventy ion microprobe analyses

471 were performed along the 7.3 mm transect and corrected to the *UWG-2* standard. The cation

472 composition of the garnet was determined adjacent to each ion microprobe pit by electron

473 microprobe, and used to correct the raw data for bias. The data were corrected using four

474 grossular standards (*GrsSE, 92W-1, 10691, AF749A)* and two intermediate grossular-

475 andradite standards (*92LEW10*, *92LEW7).* The intermediate grossular-andradite standards

476 were analyzed in the same analysis session as the zoned garnet (June 2007) and the four

477 grossular standards were analyzed in a separate session (August 2008). Instrumental biases

478 for both these sessions are reported in Table 2. *92LEW7* was analyzed during both analytical

479 sessions, and its bias relative to *UWG-2* differed by 0.03‰. Although analysis of secondary

480 garnet standards during the same analysis session is desirable, normalization to *UWG-2*

481 allows this correction to be made with a negligible change in estimated precision and

482 accuracy. Ion microprobe analyses of standards, cation compositions for each analysis point,

483   and the correction scheme used are presented in Table D and Figure B, electronic

484   supplementary materials.

485   *6.3 Results and Discussion*

486   The andradite composition of garnet 1a is plotted versus distance from the garnet rim

487   in Figure 5b. The overall pattern of chemical composition is almost identical to the traverse

488   made by Clechenko and Valley (2003, see their Fig. 5a), but was offset ca. 300 μm along

489   strike of the banding. The oxygen isotopic traverse from this study is plotted in Figure 5c,

490   superimposed on the laser fluorination data of Clechenko and Valley (2003).

491   The oxygen isotope zoning in garnet 1a measured by ion microprobe is quite well

492   correlated with that measured by laser fluorination. Two relatively andradite-rich, high-δ^{18}O

493   zones are interspersed with andradite-poor, low-δ^{18}O zones within 7300 μm of the rim (Fig.

494   5b). The ion microprobe analyses reproduce most of the laser fluorination traverse within the

495   stated uncertainty of the technique. However, ion microprobe analyses of the outermost low-

496   δ^{18}O zone yield isotope ratios up to 1‰ lower than that determined by the one laser

497   fluorination analysis at 0-1000 μm. Although it is possible that this discrepancy is due to a

498   source of bias that is unaccounted for in the correction scheme, this seems unlikely,

499   especially sine there is no indication of a hydrogrossular component in this sample Other

500   intermediate grossular composition zones in this garnet show close agreement between laser

501   and ion microprobe analyses (e.g., 4500μm from the rim), suggesting that no systematic

502   relationship between grossular and analysis misfit exists. Mixed-composition laser analyses

503   are the most likely explanation for this discrepancy.

504   Examination of this and similar garnets from Willsboro and related nearby

505   wollastonite skarns shows that the andradite bands parallel euhedral crystal faces of garnet

506   (Clechenko and Valley, 2003). In many cases, zoning is preserved in only parts of the garnet.

507   In Fig. 5a, these bands can be seen to become diffuse 3-5 mm to the left of the analysis

508   traverses because the garnet was sheared and recrystallized during granulite facies

509   metamorphism. Similar recrystallization has affected most of the garnets at Willsboro with

510   the result that their cation compositions are homogenized and that they record Sm-Nd ages

511   reset during regional metamorphism at ca. 1035 Ma (Basu et al. 1988). Taken together, all

512   data support the interpretation that zoned garnets formed at the time of contact

513   metamorphism and were locally preserved in low strain zones during recrystallization ca. 100

514   myr later. The sharp chemical zonation that parallels garnet crystal faces (Fig.5a) resulted

515   from growth zoning at 1155 Ma and is texturally and chemically distinct from the more

516   diffuse effects of granulite facies recrystallization .

517   In the unrecrystallized domains of garnet 1a, BSE imaging and electron microprobe

518   analyses reveal oscillatory zonation in Al and Fe^{3+} but not the multiple µm-scale oscillations

519   characteristic of many skarn garnets. Ion microprobe analysis of oxygen isotope ratios in this

520   garnet reveals a generally smooth profile with only two sharp changes in isotopic

521   composition (~1400 and ~5500 µm from the garnet edge). One possible reason for the

522   absence of µm-scale features is diffusional relaxation of chemical and isotopic gradients

523   during the granulite-facies regional metamorphic overprint. Clechenko and Valley (2003)

524   calculated a characteristic length scale of diffusion (distance over which 50% exchange is

525   predicted to have taken place) of 60 µm for oxygen in the Willsboro garnets based on the

526   experiments of Coghlan (1990) and a thermal event of 750˚C for 50 My, based on regional

527   thermobarometry and geochronology (Bohlen et al., 1985; McLelland et al., 2001). This

528   length-scale of homogenization is consistent with the data-set of Clechenko and Valley

529 (2003) and suggests that fine-scale chemical features were homogenized in the Willsboro

530 garnets, and only mm-scale zonation was preserved through granulite-facies metamorphism.

531   The most important feature of the new ion microprobe data for $\delta^{18}O$ is the sharp

532 gradient between the outermost low-$\delta^{18}O$ rim and high-$\delta^{18}O$ zone between 1377 to 1393 μm

533 from the edge of the garnet (Fig. 5c). This transition represents a jump of 2.1‰ in 16 μm

534 (measured from the center of the analysis pits) coincident with an equally sharp change in the

535 andradite content of garnet visible in the back-scattered electron image in Figure 6a.

536 Although $\delta^{18}O$ decreases gradually across the Fe-rich band from a maximum of 6.3‰ at

537 2400μm to 4.2 ‰ at 1400μm, the oxygen isotope ratios measured in the outermost grossular-

538 rich zone are constant at 1.8‰ (Fig. 5c). If the gradual decrease in $\delta^{18}O$ within the more

539 andradite-rich band were the result of diffusional relaxation after garnet growth across an

540 original step-change in $\delta^{18}O$ at 1380 μm, a symmetrical increase in $\delta^{18}O$ would occur in the

541 adjacent grossular-rich zone approaching 1380 μm. No gradual change is seen from 500 to

542 1380 μm and thus the smooth changes in $\delta^{18}O$ within the andradite-rich band are interpreted

543 as growth-zoning, as is the sharp 2.1‰ gradient at 1380μm between these two zones.

544 The preservation of a sharp gradient in ™^{18}O at 1380 ⌈m provides a very tight constraint on

545 the maximum amount of oxygen diffusion in this garnet throughout its entire history. There

546 is no diffusional process that would sharpen a $\delta^{18}O$ gradient, once formed. Thus, the

547 maximum amount of oxygen exchange can be estimated if the gradient is assumed to have

548 formed as a step of 2.1‰ over 0μm. This is a boundary condition, and it is possible that

549 garnet growth produced a more gradual profile, closer to that observed in this garnet. If this

550 were the case, models based on an initial step condition will over-estimate the duration of the

551 metamorphic event or rate of exchange.

552   Diffusion of oxygen across this boundary was modeled as a simple, 1-dimensional

553   system using equation 3.45 of Crank (1975). Because of the small scale of diffusion (<

554   16μm) compared to the size of the garnet (> 1 cm), the 1-D model is a conservative

555   approximation. Initial values for core and rim $\delta^{18}O$ were taken as the average of ion

556   microprobe data within 100 µm of the transition (4.3±0.4‰ and 1.8±0.5‰, respectively).

557   The sharp Fe^{3+}/Al and $\delta^{18}O$ transition boundary at 1380 ⌠m is shown in back-scattered

558   electron imaging in Figure 6a and analysis pits are labeled in $\delta^{18}O$ VSMOW. A detail of the

559   ion-microprobe traverse in this region is shown in Figure 6b with modeled diffusion curves

560   superimposed on the data. At 750˚C, the diffusion rate (D) of oxygen in garnet based the

561   experiments of Coghlan (1990, $P_{H2O} = 1$ kbar) is estimated at $4.2x10^{-25}m^2s^{-1}$. At this rate, the

562   observed step could only have survived a thermal event of less than 1 My. Furthermore, this

563   calculation does not include the effects of diffusion that would have also occurred during the

564   heating and cooling of regional metamorphism. The extremely rapid heating and cooling

565   required by the sharp gradient in this garnet interpreted in the context of the experiments of

566   Coghlan (1990) are in striking contrast to the slow cooling rates of ~ 1.5˚C/My reported by

567   Mezger et al. (1991) for this region. Although fleeting thermal events have recently been

568   proposed for regional metamorphism (e.g., Ague and Baxter, 2007), it seems unlikely that the

569   mid-crustal, 7-8 Kb granulite-facies regional metamorphism of the Adirondack Highlands

570   could have taken place over so short a time span. Coghlan (1990) reports a conservative error

571   envelope for the diffusion coefficient used in this calculation and even at the extreme, the

572   slowest value of D within this range (i.e., the lowest value of D_o and the highest value of E_A)

573   is not consistent with a peak of metamorphism lasting as long as 50 Myr. Taken together, the

574   experimental data and the measured gradient for $\delta^{18}O$ (Fig. 6b) are most consistent with a

575 thermal peak lasting less than 5 My. If these estimates of the diffusion rate of oxygen in

576 garnet at 750^oC are correct, then the peak of regional metamorphism in the NE Adirondack

577 Highlands was significantly faster than has previously been assumed. With increased

578 understanding of the diffusion rate of oxygen in garnet and with further ion microprobe

579 studies of single crystals, time and rate estimates based on oxygen diffusion profiles in garnet

580 (and other minerals) will become more accurate than presently possible.

581 New technology and techniques used in the analysis of oxygen isotopes by ion

582 microprobe have greatly improved the precision of the technique in the analysis of phases

583 with limited solid solution. The use of a single garnet standard mounted in samples, regularly

584 analyzed as a monitor for changes in instrumental conditions, provides similar precision in

585 the analysis of garnets. The correction of instrumental bias due to cation composition in

586 garnets can be done readily using 3 or more compositional standards in a separate standard

587 mount. A correction scheme based on the grossular content of pyralspite garnets and the

588 andradite content of ugrandite garnets brings the accuracy of analyses to the same order as

589 analytical precision with a combined uncertainty of $\pm$ 0.5 to 0.6‰, 2 S.D. Application of this

590 approach to garnets will have widespread utility for estimation of thermal and fluid history

591 during metamorphism.

592

603

604

References

606 Afifi, A.M. and Essene, E.J. (1988) Minfile: a microcomputer program for storage and
607   manipulation of chemical data on minerals. Am. Mineral., 73: 446-448.
608 Ague, J.J. and Baxter, E.F. (2007) Brief thermal pulses during mountain building recorded by
609   Sr diffusion in apatite and multicomponent diffusion in garnet. Earth and Planet. Sci.
610   Lett., 261: 500-516
611 Basu, A.R., Faggert, B.E., and Sharma, M., 1988. Sm-Nd isotopic study of wollastonite
612   skarn and garnet amphibolite metamorphism in the Adirondack Mountains, New
613   York. *EOS*, 69: 468.
614 Bohlen, S.R., Valley, J.W. and Essene, E.J., 1985. Metamorphism in the Adirondacks: I,
615   Petrology, pressure and temperature. J. Pet., 26(4): 971-992.
616 Bowman, J.R., 1998. Stable-isotope systematics of skarns. In: D.R. Lentz, Editor,
617   Mineralized Intrusion-Related Skarn Systems, Mineral. Assoc. Can. Short Course
618   Vol. 26, Mineralogical Association of Canada: 99–145.
619 Cavosie, A.J., Valley, J.W., Wilde, S.A. and EIMF, 2005. Magmatic $\delta^{18}O$ in 4400-3900 Ma
620   detrital zircons: A record of the alteration and recycling of crust in the Early Archean.
621   Earth Plan. Sci. Lett., 235: 663-81.
622 Clechenko, C.C. and Valley, J.W., 2003. Oscillatory zoning in garnet from the Willsboro
623   wollastonite skarn, Adirondack Mts, New York: a record of shallow hydrothermal
624   processes preserved in a granulite facies terrane. J. Meta. Geol., 21: 771-784.
625 Coghlan, R. A., 1990. Studies in diffusional transport: Grain boundary transport of oxygen in
626   feldspars, diffusion of oxygen, strontium, and the REE's in garnet, and the thermal
627   histories of granitic intrusions in south-central Maine using oxygen isotopes. PhD
628   Thesis, Brown University. Providence, RI.
629 Crank, J., 1975. The Mathematics of Diffusion. Oxford University Press, New York, 414 pp.
630 Crowe, D.E., Riciputi, L.R., Bezenek, S. and Ignatiev, A., 2001. Oxygen isotope and trace
631   element zoning in hydrothermal garnets: windows into large-scale fluid-flow
632   behavior. Geology, 29: 479-482.
633 Diella, V., Sani, A., Levy, D. and Pavese, A., 2004. High-pressure synchrotron X-ray
634   diffraction study of spessartine and uvarovite: A comparison between different
635   equation of state models. Am. Mineral., 89: 371-376.
636 Donovan, J.J., Kremser, D. and Fournelle, J.H. (Editors), 2007. Probe for Windows User's
637   Guide and Reference, Enterprise Edition, 355 pp.
638 Eiler, J.M., Graham, C.M. and Valley, J.W., 1997. SIMS analysis of oxygen isotopes; matrix
639   effects in complex minerals and glasses. Chem. Geol., 138: 221-244.
640 Elsenheimer, D. and Valley, J.W., 1993. Submillimeter scale zonation of $\delta^{18}O$ in quartz and
641   feldspar, Isle-of-Skye, Scotland. Geochim. Cosmochim. Acta, 57: 3669-3676.
642 Ford, F., 1987. Petrology and geochemistry of xenoliths from the Blaauwbosch kimberlite
643   pipe, R.S.A., Undergraduate Thesis, University of Toronto, Toronto.
644 Garlick, G.D., Macgregor, I.D. and Vogel, D.E., 1971. Oxygen isotope ratios in eclogites
645   from kimberlites. Science, 172: 1025-1027.

646   Gnaser, H., 2008. Isotopic fractionation of sputtered anions: C^- and C_2^-. Nuc. Instr. & Meth.
647   Phys. Res, Sect. B. 266: 37-43.
648   Hervig, R.L., Williams, P., Thomas, R.M., Schauer, S.N. and Steele, I.M., 1992.
649   Microanalysis of oxygen isotopes in insulators by secondary ion mass spectrometry.
650   Int. J. Mass Spectrom. Ion Proc., 120: 45-63.
651   Huberty JM, Kita NT, Heck PR, Kozdon R, Fournelle JH, Xu H and Valley JW (2009)
652   Crystal orientation effects on bias of $\delta^{18}O$ in magnetite by SIMS. Goldschmidt
653   Conference, Geochim. Cosmochim. Acta v.73:13S, A562.
654   Jamtveit, B., Wogelius, R.A. and Fraser, D.G., 1993. Zonation Patterns of Skarn Garnets -
655   Records of Hydrothermal System Evolution. Geology, 21: 113-116.
656   Jamtveit, B. and Hervig, R.L., 1994. Constraints on transport and kinetics in hydrothermal
657   systems from zoned garnet crystals. Science, 263: 505-508.
658   Kelly, J.L., Fu, B., Kita, N.T. and Valley, J.W., 2007. Optically continuous silcrete quartz
659   cements of the St. Peter Sandstone: High precision oxygen isotope analysis by ion
660   microprobe. Geochim. Cosmochim. Acta, 71: 3812-3832.
661   Kita, N.T., Ushikubo, T., Fu, B. and Valley, J.W., 2009 High precision SIMS oxygen isotope
662   analyses and the effect of sample topography. Chem. Geol.,
663   doi:10.1016/j.chemgeo.2009.02.012.
664   Kohn, M.J. and Valley, J.W., 1998. Effects of cation substitutions in garnet and pyroxene on
665   equilibrium oxygen isotope fractionations. J. Meta. Geol., 16: 625-639.
666   Kohn, M.J., Valley, J.W., Elsenheimer, D. and Spicuzza, M.J., 1993. Isotope zoning in garnet
667   and staurolite; evidence for closed-system mineral growth during regional
668   metamorphism. Am. Mineral., 78: 988-1001.
669   Kohn, M.J. and Valley, J.W., 1994. Oxygen isotope constraints on metamorphic fluid flow,
670   Townshend Dam, Vermont, USA. Geochim. Cosmochim. Acta, 58: 5551-5566.
671   Kohn, M.J., Spear, F.S. and Valley, J.W., 1997. Dehydration-melting and fluid recycling
672   during metamorphism: Rangeley Formation, New Hampshire, USA. J. Petrol., 38:
673   1255-1277.
674   Lancaster PJ, Fu B, Page FZ, Kita NT, Bickford ME, Hill BM, McLelland JM, Valley JW
675   (2009) Genesis of metapelitic migmatites in the Adirondack Mts., New York, J Meta
676   Geol, 27: 41-54.
677   McLelland, J., Hamilton, M., Selleck, B., McLelland, J., Walker, D. & Orrell, S., 2001.
678   Zircon U-Pb geochronology of the Ottawan Orogeny, Adirondack Highlands, New
679   York: regional and tectonic implications. Precamb. Res., 109, 39–72.
680   McLelland, J.M., Bickford, M.E., Hill, B.M., Clechenko, C.C., Valley, J.W. and Hamilton,
681   M.A., 2004. Direct dating of Adirondack Massif anorthosite by U-Pb SHRIMP
682   analysis of igneous zircon; implications for AMCG complexes. Geol. Soc. Am. Bull.,
683   116(11-12): 1299-1317.
684   MacGregor, I.D. and Manton, W.I., 1986. Roberts Victor eclogites: Ancient oceanic crust. J.
685   Geophys. Res., 91: 14,063-14,079.
686   Martin, L., Duchêne, S., Deloule, E. and Vanderhaeghe, O., 2006. The isotopic composition
687   of zircon and garnet: A record of the metamorphic history of Naxos, Greece. Lithos,
688   87: 174-192.
689   Mezger, K., Rawnsley, C., Bohlen, S.R. and Hanson, G.N., 1991. U-Pb garnet, sphene,
690   monazite, and rutile ages: Implications for the duration of high grade metamorphism
691   and cooling histories, Adirondack Mts., New York. J. Geol., 99: 415-428.

692   Novak, G. and Gibbs, G.V., 1971. The crystal chemistry of silicate garnets. Am Mineral., 56:
693   791-825.
694   Page, F.Z., Ushikubo, T., Kita, N.T., Riciputi, L.R. and Valley, J.W., 2007. High-precision
695   oxygen isotope analysis of picogram samples reveals 2 μm gradients and slow
696   diffusion in zircon. Am. Mineral., 92: 1772-1775.
697   Peck, W.H. and Valley, J.W., 2004. Quartz-garnet isotope thermometry in the south
698   Adirondack Highlands (Grenville Province, New York). J. Meta. Geol., 22: 763-773.
699   Peck, W.H., Valley, J.W. and Graham, C.M., 2003. Slow oxygen diffusion rates in igneous
700   zircons from metamorphic rocks. Am. Mineral., 88: 1003-1014.
701   Riciputi, L.R. and Paterson, B.A., 1994. High spatial-resolution measurement of O isotope
702   ratios in silicates and carbonates by ion microprobe. Am. Mineral., 79: 1227-1230.
703   Riciputi, L.R., Paterson, B.A. and Ripperdan, R.L., 1998. Measurement of light stable
704   isotope ratios by SIMS:: Matrix effects for oxygen, carbon, and sulfur isotopes in
705   minerals. Int. J. Mass Spectrom., 178: 81-112.
706   Robie, R.A. and Hemingway, B.S., 1995. Thermodynamic properties of minerals and related
707   substances at 298.15 K and 1 bar (10^5 Pascals) pressure and at higher temperatures. B
708   2131, U. S. Geological Survey, Reston.
709   Schulze, D.J., Valley, J.W. and Spicuzza, M.J., 2003. The oxygen isotope composition of
710   mantle eclogites, 8th International Kimberlite Conference, Victoria, B.C.
711   Shimizu, N. and Hart, S.R., 1982. Isotope Fractionation in Secondary Ion Mass-
712   Spectrometry. J. App. Phys. 53: 1303-1311.
713   Skelton, A., Annersten, H. and Valley, J., 2002. $\delta^{18}O$ and yttrium zoning in garnet: time
714   markers for fluid flow? J. Meta. Geol., 20: 457-466.
715   Taylor, B.E. and O'Neil, J.R., 1977. Stable isotope studies of metasomatic Ca-Fe-Al-Si
716   skarns and associated metamorphic and igneous rocks, Osgood Mountains, Nevada.
717   Contrib. Mineral. Petrol., 63: 1-49.
718   Valley, J.W., 1985. Polymetamorphism in the Adirondacks: Wollastonite at contacts of
719   shallowly intruded anorthosite. In: A.C. Tobi and L.R. Touret Jacques (Editors), The
720   Deep Proterozoic Crust in the North Atlantic Provinces. Reidel, Dordrecht, pp. 217-
721   236.
722   Valley, J.W., 1986. Stable isotope geochemistry of metamorphic rocks. In: J.W. Valley, H.P.
723   Taylor and J.R. O'Neil (Editors), Stable isotopes in high temperature geological
724   processes. Rev. Mineral., Vol. 16, pp. 445-489.
725   Valley J.W. and Kita N.T. (2009) *In situ* Oxygen Isotope Geochemistry by Ion Microprobe,
726   In: Fayek M. (ed) GAC/MAC Short Course: Secondary Ion Mass Spectrometry in the
727   Earth and Planetary Sciences, 41:19-63.
728   Valley, J.W. and Graham, C.M., 1991. Ion microprobe analysis of oxygen isotope ratios in
729   granulite facies magnetites; diffusive exchange as a guide to cooling history. Contrib.
730   Mineral. Petrol., 109: 38-52.
731   Valley, J.W. and O'Neil, J.R., 1982. Oxygen isotope evidence for shallow emplacement of
732   Adirondack anorthosite. Nature, 300: 497-500.
733   Valley, J.W., Bohlen, S.R., Essene, E.J. and Lamb, W., 1990. Metamorphism in the
734   Adirondacks: II, The role of fluids. J. Petrol., 31(3): 555-596.
735   Valley, J.W., Kitchen, N., Kohn, M.J., Niendorf, C.R. and Spicuzza, M.J., 1995. UWG-2, a
736   garnet standard for oxygen isotope ratios: strategies for high precision and accuracy
737   with laser heating. Geochim. Cosmochim. Acta, 59: 5223-5231.

738 Vielzeuf, D., Champenois, M., Valley, J.W., Brunet, F. and Devidal, J.L., 2005a. SIMS
739   analyses of oxygen isotopes: Matrix effects in Fe-Mg-Ca garnets. Chem. Geol., 223:
740   208-226.
741 Vielzeuf, D., Veschambre, M. and Brunet, F., 2005b. Oxygen isotope heterogeneities and
742   diffusional profiles in composite metamorphic/magmatic garnets from the Pyrenees.
743   Am. Mineral., 90: 463-472.
744 Yardley, B.W.D., Rochelle, C.A., Barnicoat, A.C. and Lloyd, G.E., 1991. Oscillatory zoning
745   in metamorphic minerals - an indicator of infiltration metasomatism. Mineral. Mag.,
746   55: 357-365.
747

748 **Figure Captions**

749

750 Figure 1. Cation compositions of garnet standards used in this study. Standards used in
751   previous studies are keyed to the study of their first use.

752

753 Figure 2. Instrument bias for oxygen isotope analysis at WiscSIMS (‰ relative to UWG-2)
754   as a function of cation composition of garnet standards expressed in terms of mol %
755   garnet end-members. (a) Bias in Al-rich Mg-Fe^{2+}-Ca-Mn garnets is correlated with
756   grossular content (CaAl). (b) Bias in Ca- rich Al-Fe^{3+} garnets is inversely correlated
757   with grossular. MexGrs is poorly calibrated, see text.

758

759 Figure 3. Instrument bias for oxygen isotope analysis at WiscSIMS ($\delta^{18}O$, ‰ relative to
760   UWG-2) as a function of calculated molar volume of the garnet standards. Errors are
761   plotted as 2 S.E. The line is a least-squares linear regression (equation 5.1) and yields
762   an R^2 value of 0.95. Two garnets (*MexGrs* and *SpsSE*) fall outside of 2 S.E. of the
763   estimate.

764

765 Figure 4. Instrument bias for oxygen isotope analysis at WiscSIMS ($\delta^{18}O$, ‰ relative to
766   UWG-2) as a function of Ca-rich garnet end-members. Instrumental bias in Al-rich
767   pyralspite garnets (plotted as open circles) increases with grossular + uvarovite
768   content. Instrumental bias in Ca-rich ugrandite garnets (plotted as filled circles) is
769   greater than that in pyralspite garnets and increases with andradite + CaTi garnet
770   content. Sample *MexGrs* is poorly calibrated, see text. Error bars are 2 S.E. of
771   multiple analyses and are smaller than the sample points in most cases. The low-
772   andradite grossular sample *GrsSE* appears in both plots. The polynomial best fit
773   curves (equations 5.2 and 5.3) are also shown.

774

775 Figure 5. Oscillatory-zoned skarn garnet from the granulite-facies Willsboro wollastonite
776   skarn, Adirondack Mountains, New York, USA. (a) Fe-Kα X-ray image of the garnet
777   showing andradite-rich zones (purple) and grossular-rich zones (blue). Yellow and
778   orange minerals are sphene and feldspar. The location of the $\delta^{18}O$ analyses by laser
779   fluorination (Clechenko and Valley, 2003) are shown as a thick black line, the
780   location of the ion microprobe traverse in this study is shown as a thick white line. (b)
781   mol % andradite determined by electron microprobe vs. distance from garnet edge
782   (top of figure). (c) traverses of $\delta^{18}O$, open symbols represent ion microprobe analyses
783   with ± 0.6‰ error bars that represent both the precision and accuracy of the

784   technique, black bars are the laser fluorination data of mg-size samples by Clechenko
785   and Valley (2003).
786

787   Figure 6. Sharp $\delta^{18}O$ and cation discontinuity 1377 μm from the garnet edge (a) High-
788   contrast back-scattered electron image of the sharp andradite-grossular transition
789   within the garnet. Ion microprobe pits (10 μm dia.) are labeled with $\delta^{18}O$ ‰
790   VSMOW. (b) detail of $\delta^{18}O$ traverse over the same field of view with simulated
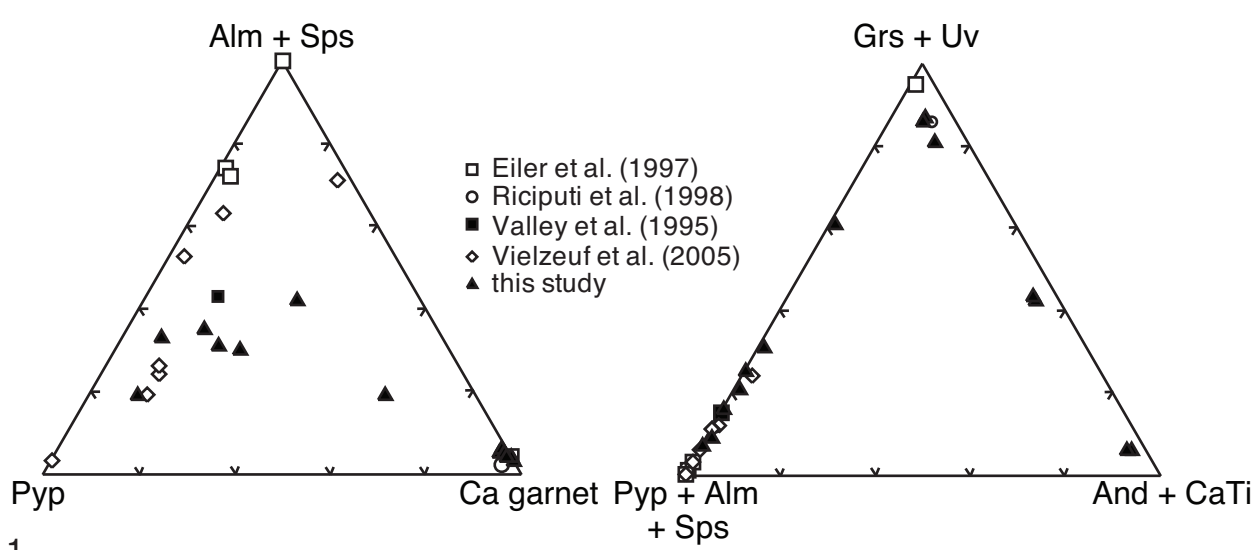791   diffusion profiles (see text).
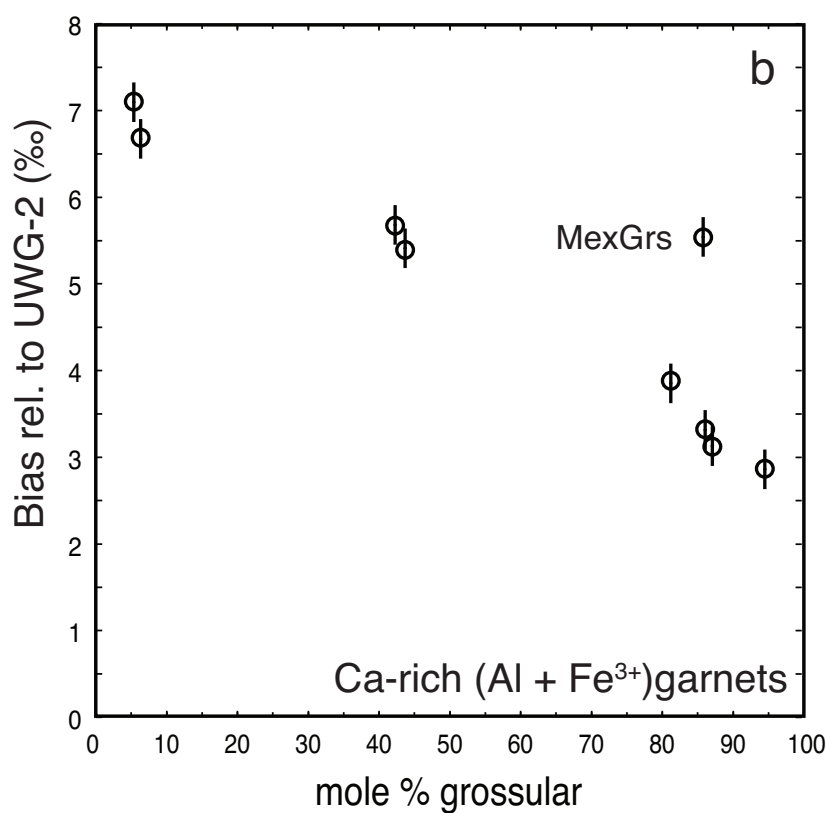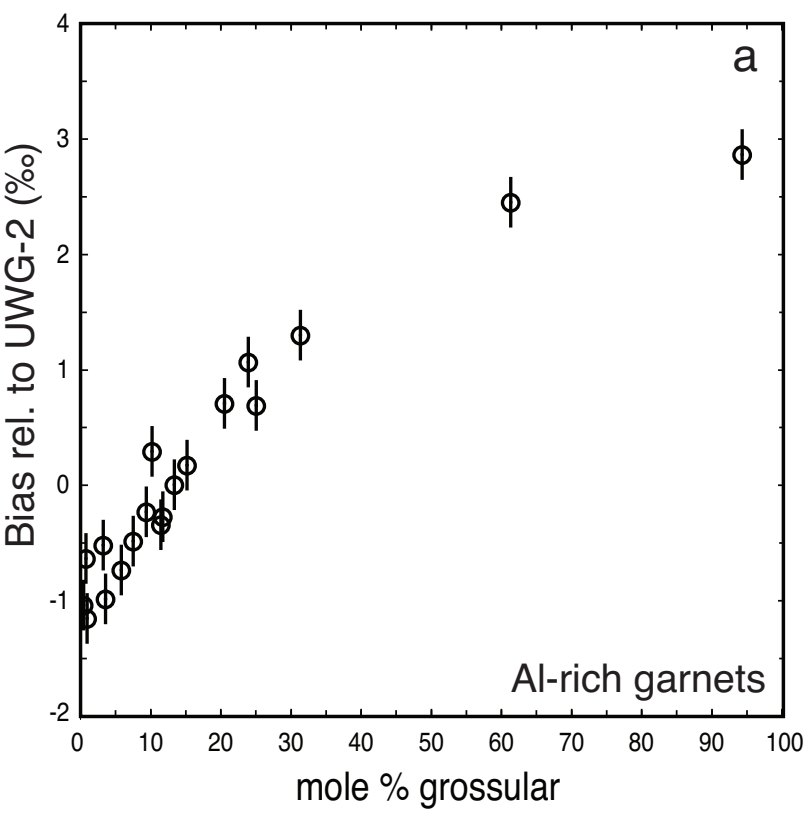792
793

Figure 1

Fig. 1

Figure 2

Figure 3

Figure 4

Fig. 4

Figure 5

a

3 mm

Fe Kα
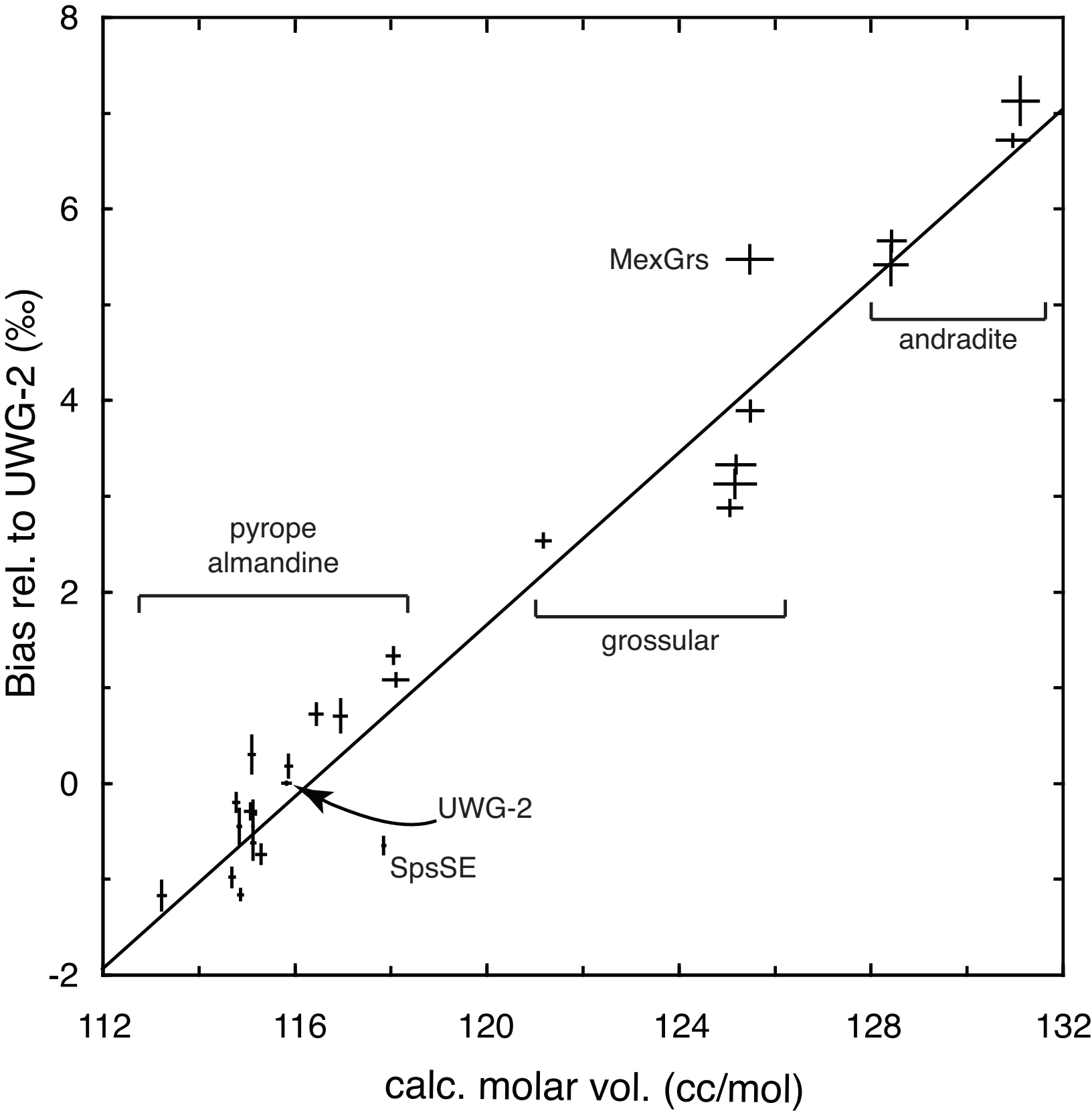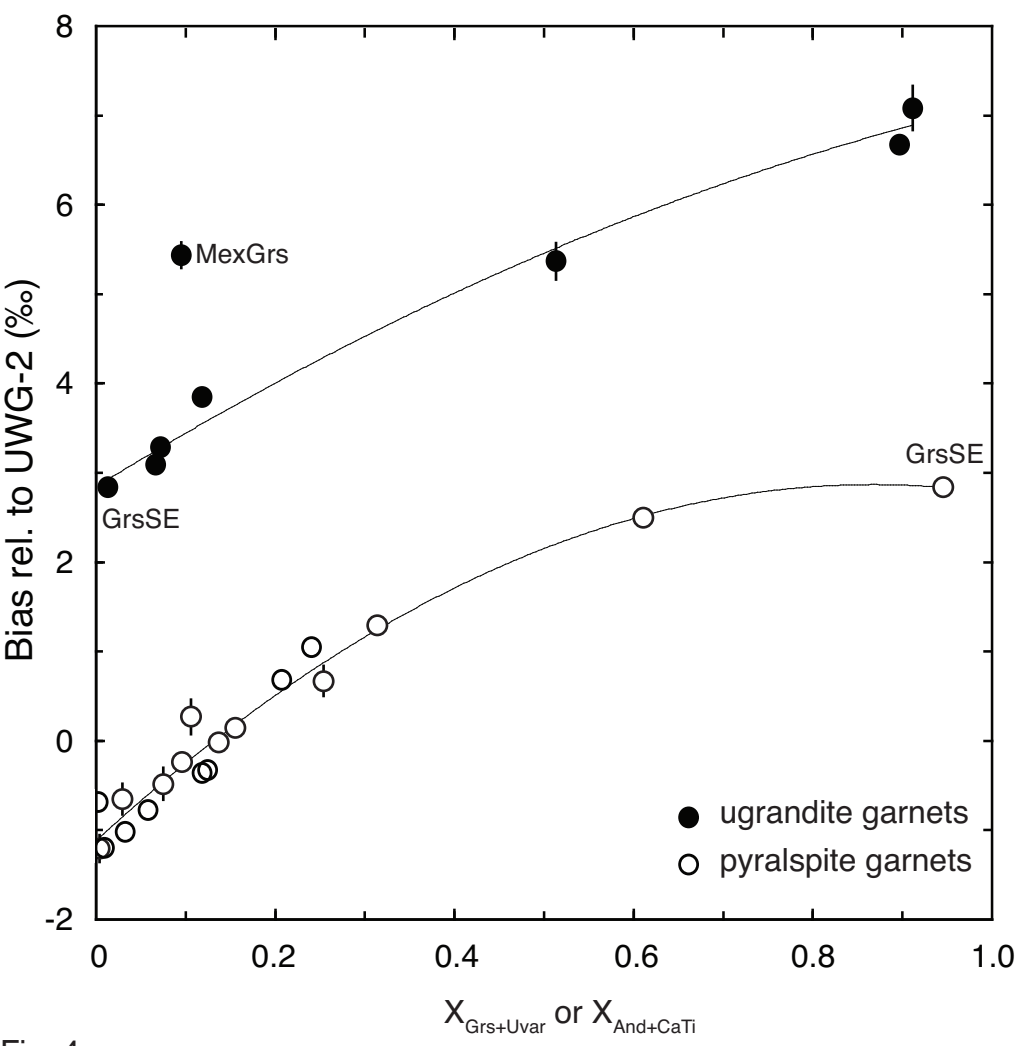
Clechenko & Valley (2003)
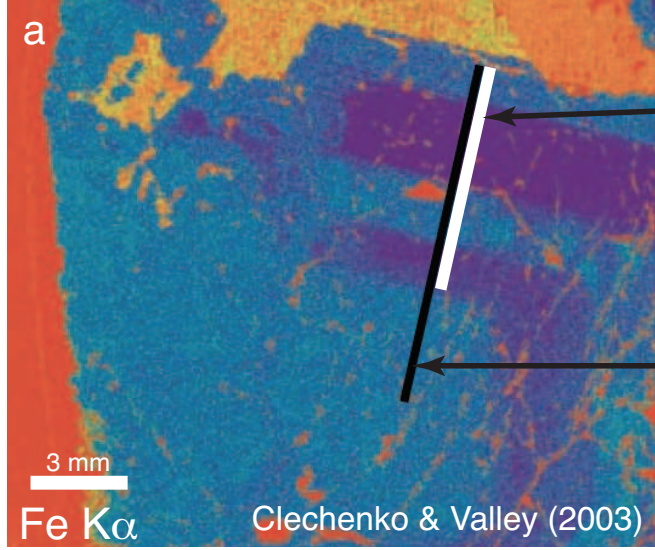
Location of electron- and ion-microprobe traverses shown in (b) and (c).

Location of the laser fluorination δ18O traverse made by Clechenko & Valley (2003). Data collected immediately adjacent to the traverse made in this study is shown in (c).

b

mole % andradite

c

$\delta^{18}O_{Grt}$ (‰, VSMOW)

rim

core

Laser fluorination

Ion microprobe

distance from rim (μm)

Fig. 5

Figure 6

a

Grs(CaAl)-rich rim

1.8‰

1.6‰

2.1‰

4.2‰

4.4‰

4.0‰

And(CaFe³⁺)-rich band

4.5 ‰

4.2‰

BSE 50 μm

4.7‰

b

Model diffusion curves
4.2x10⁻²⁵m²/s, 50 My
4.2x10⁻²⁵m²/s, 5 My

$\delta^{18}O_{Grt}$ (‰, VSMOW)

distance from rim (μm)
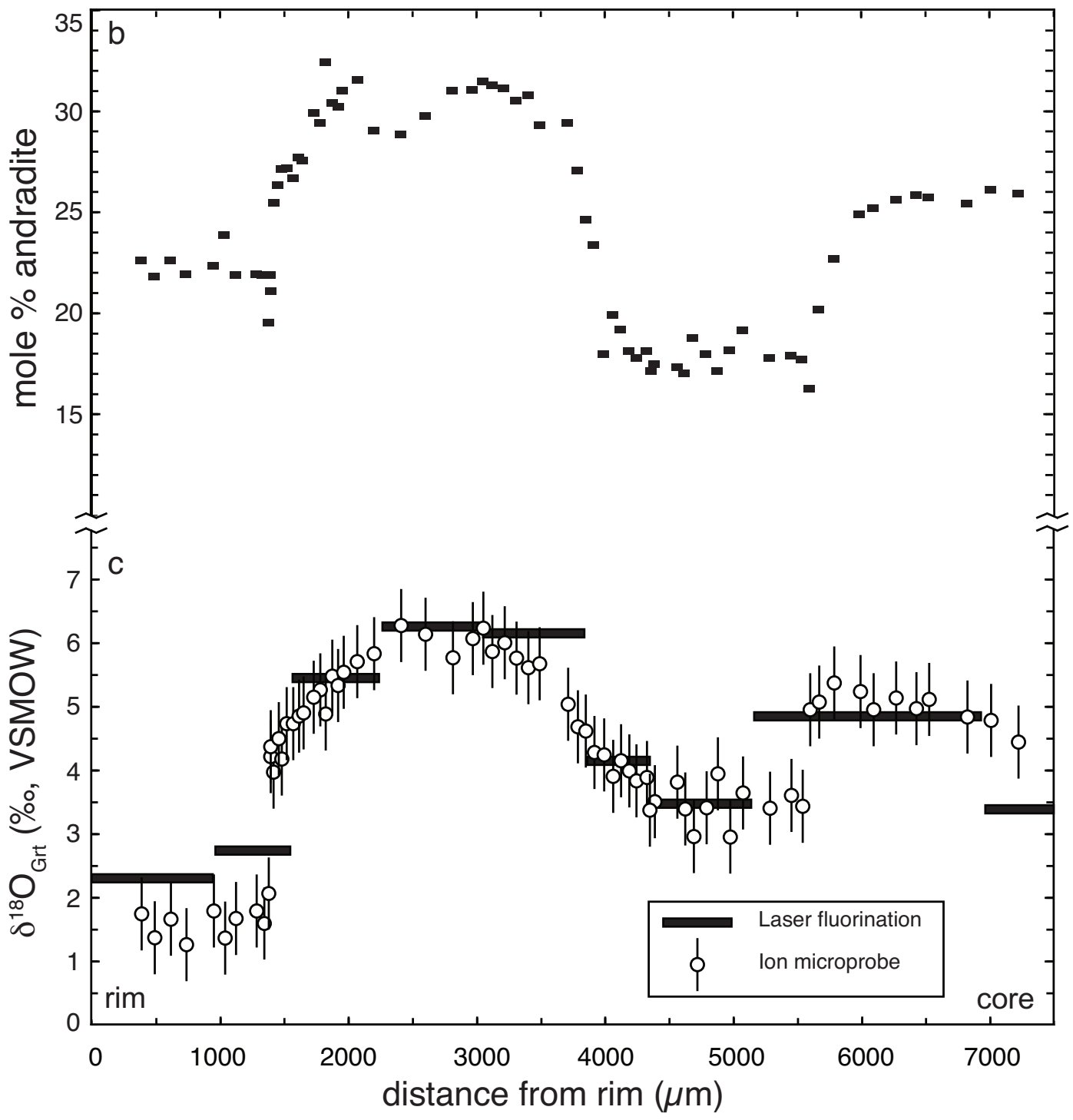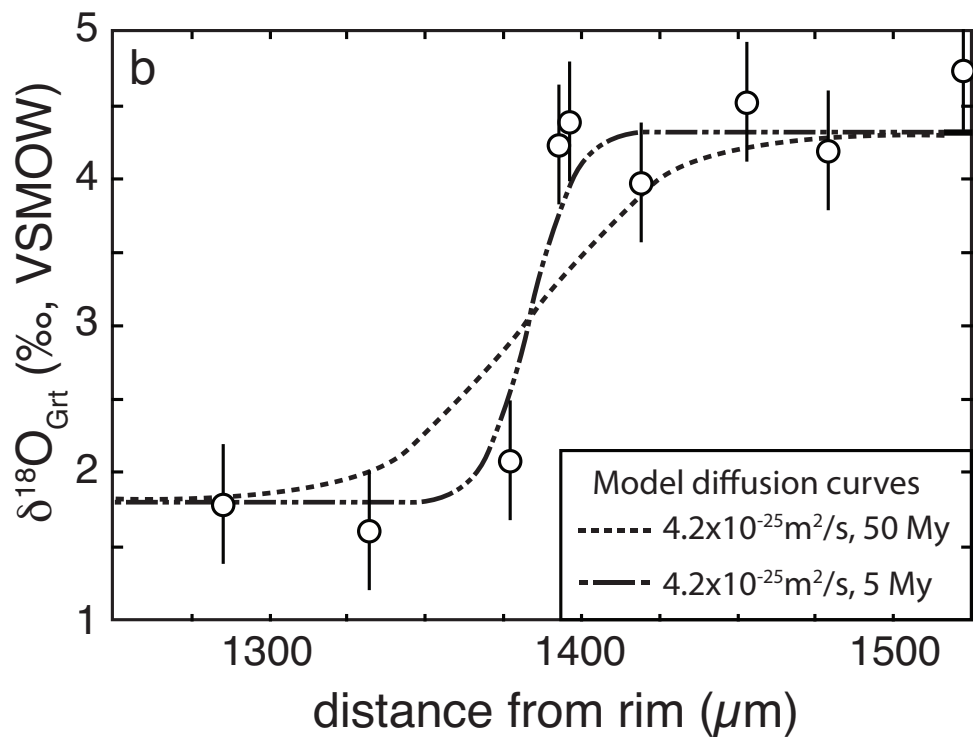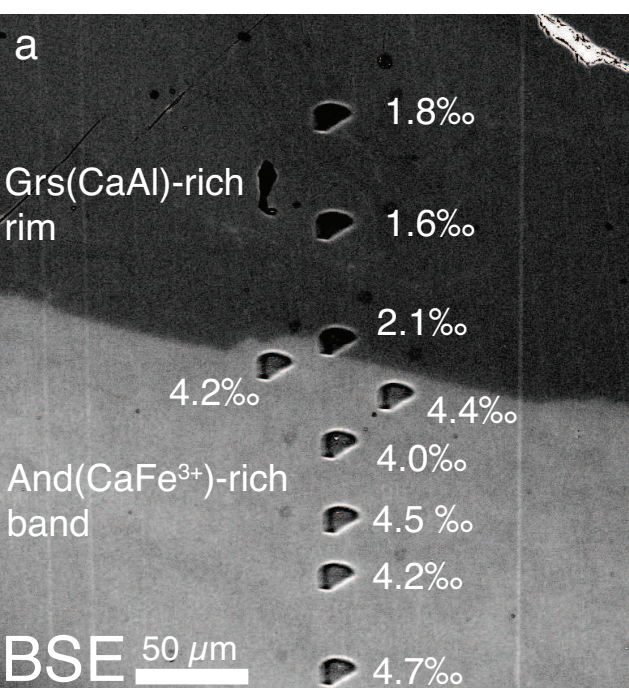
Fig. 6

Table 1. Garnet standards analyzed for $\delta^{18}O$ at WiscSIMS

Standard	Average composition	Calculated Molar V[1]	2 S.D.[1]	$\delta^{18}O$[2] (‰ VSMOW)	Average[3] $\delta^{18}O*$	Average bias ‰ rel. UWG-2	2 S.D.[4]	n[4]	2 S.E.[4]	Ref.[5]
Pyrope										
PypDM	$Pyp_{97}Alm_3$	113.2	0.07	5.60	4.42	-1.18	0.73	23	0.15	(6)
13-63-19	$Pyp_{71}Alm_{18}Grs_9Sps_2$	114.8	0.05	5.92	5.71	-0.21	0.29	10	0.09	(5)
PypAA	$Pyp_{69}Alm_{18}Grs_{11}Sps_1Uv_1$	115.1	0.10	5.50	5.20	-0.30	0.25	10	0.08	(6)
PypAK	$Pyp_{64}Alm_{24}Grs_{11}Sps_1$	115.1	0.05	5.50	5.17	-0.33	0.42	10	0.13	(6)
PypMM	$Pyp_{63}Alm_{25}Grs_{11}Sps_1$	115.1	0.05	5.30	5.59	0.29	0.60	10	0.19	(6)
13-62-29	$Pyp_{59}Alm_{32}Grs_8Sps_1$	114.9	0.03	7.39	6.93	-0.46	0.56	10	0.18	(5)
13-62-27	$Pyp_{49}Alm_{35}Grs_{15}Sps_1$	115.9	0.06	6.49	6.66	0.17	0.36	10	0.11	(5)
13-63-20	$Pyp_{48}Alm_{31}Grs_{20}Sps_1$	116.5	0.12	6.14	6.85	0.71	0.34	10	0.11	(5)
13-63-44	$Pyp_{45}Alm_{29}Grs_{25}Sps_1$	117.0	0.12	6.37	7.06	0.69	0.53	10	0.17	(5)
Almandine										
AlmSE	$Alm_{74}Pyp_{25}Grs_1$	114.9	0.03	8.30	7.13	-1.17	0.31	38	0.05	(2), (6)
AlmCMG	$Alm_{70}Pyp_{25}Grs_3Sps_2$	115.1	0.03	7.50	6.87	-0.63	0.65	14	0.17	(2), (6)
2B3	$Alm_{67}Grs_{24}Sps_4Pyp_3And_2$	118.1	0.26	6.90	7.97	1.07	0.35	30	0.06	(6)
Beta114	$Alm_{61}Pyp_{31}Grs_6Sps_2$	115.3	0.09	9.30	8.55	-0.75	0.45	30	0.08	(6)
Bal509	$Alm_{52}Pyp_{44}Grs_3Sps_1$	114.7	0.04	12.30	11.31	-0.99	0.30	10	0.09	(6)
UWG-2	$Alm_{45}Pyp_{40}Grs_{14}Sps_1$	115.8	0.08	5.80	5.80	0.00	0.35	357	0.02	(1), (2), (6)
13-63-21	$Alm_{41}Grs_{31}Pyp_{27}Sps_1$	118.1	0.12	4.55	5.87	1.32	0.30	14	0.08	(5)
Spessartine										
SpsSE	$Sps_{94}Alm_6$	117.9	0.02	5.40	4.74	-0.66	0.36	19	0.08	(2), (6)
Grossular										
GrsSE	$Grs_{94}Alm_4Sps_1CaTi_1$	125.1	0.24	3.80	6.66	2.86	0.48	37	0.08	(2), (6)
92W-1	$Grs_{87}And_5Alm_5Pyp_2CaTi_1$	125.2	0.42	-0.34	2.77	3.11	0.63	20	0.14	(4)
10691	$Grs_{86}And_5Alm_5Pyp_2CaTi_2$	125.2	0.40	0.18	3.49	3.31	0.28	10	0.09	(4)
MexGrs	$Grs_{86}And_8Pyp_3Alm_1Sps_1CaTi_1$	125.5	0.47	10.60	16.05	5.45	0.67	22	0.14	(3)
AF749A	$Grs_{81}And_{10}Alm_5Pyp_1Sps_1CaTi_2$	125.5	0.26	-1.24	2.63	3.87	0.32	10	0.10	(4)
R-53	$Grs_{61}Alm_{19}Pyp_{19}CaTi_1$	121.2	0.14	5.33	7.85	2.52	0.15	5	0.07	(5)
Andradite										
92LEW2	$And_{91}Grs_6Alm_3$	131.1	0.37	-1.47	5.63	7.10	0.78	10	0.25	(4)
92LEW7	$And_{89}Grs_6Alm_4Pyp_1$	131.0	0.33	-1.60	5.09	6.69	0.25	18	0.06	(4)
92LEW10	$And_{50}Grs_{42}Alm_4CaTi_2Pyp_2$	128.4	0.28	-1.20	4.44	5.64	0.38	14	0.10	(4)
92LEW8	$And_{49}Grs_{43}Alm_4CaTi_3Pyp_1$	128.4	0.34	-0.93	4.46	5.39	0.64	10	0.20	(4)

[1] (cm^3/mol) calculated from compositional data, see text, [2] Values of $\delta^{18}O$ were calibrated against the VSMOW scale using UWG-2 by laser fluorination and gas-source mass spectrometry, see text. [3] Average raw value measured by ion microprobe, corrected to UWG-2, [4] Variability measured by ion probe.
[5] (1) Valley et al. (1995), (2) Eiler et al. (1997), (3) Riciputi et al. (1998), (4) Kohn & Valley (1998), (5) Schulze et al. (2003), (6) Vielzeuf et al. (2005)

Table 2
Click here to download Table: Table 2.pdf

Table 2. Instrument bias of each garnet standard relative to UWG-2 over a 28 month period

Standard	Apr-06	Aug-06	Sep-06	Nov-06	Jan-07	Apr-07	Jun-07	Aug-08	Avg.	Range
				Bias relative to UWG-2 (‰)						
Pyrope										
PypDM	-1.5	-1.1			-0.9	-0.8			-1.1	0.7
13-63-19	-0.2								-0.2	
PypAA	-0.3								-0.3	
PypAK	-0.3								-0.3	
PypMM	0.3								0.3	
13-62-29	-0.5								-0.5	
13-62-27	0.2								0.2	
13-63-20	0.7								0.7	
13-63-44	0.7								0.7	
Almandine										
AlmSE	-1.2	-1.1	-1.2	-1.0	-1.2			-1.2	-1.1	0.2
AlmCMG	-0.5							-0.9	-0.7	0.4
2B3	1.1	1.1	1.0		1.0				1.1	0.2
Beta114	-0.9		-0.7	-0.7	-0.5				-0.7	0.4
Bal509	-1.0								-1.0	
UWG-2	0.0								0.0	
13-63-21	1.3		1.3						1.3	0.0
Spessartine										
SpsSE	-0.7	-0.6			-0.6				-0.6	0.1
Grossular										
GrsSE	2.7	2.8	2.9		2.8	3.2		3.2	2.9	0.5
92W-1								3.1	3.1	
10691								3.3	3.3	
MexGrs	5.6						5.5	5.0	5.4	0.6
AF749A								3.9	3.9	
R-53	2.4	2.5							2.4	0.2
Andradite										
92LEW2	7.1								7.1	
92LEW7	6.7						6.6	6.6	6.7	0.1
92LEW10	5.6						5.7		5.7	0.1
92LEW8	5.4								5.4	